Modeling and estimating acoustic transfer functions of external ears with or without headphones

Huiqun Deng[a] and Jun Yang
Institute of Acoustics, Chinese Academy of Sciences, Beijing 100190, China

(Received 17 February 2015; revised 25 June 2015; accepted 26 June 2015; published online 10 August 2015)

The acoustic transfer functions of external ears with or without headphones affect the features of perceived sounds and vary considerably with listeners and headphones. A method for estimating the frequency responses of external-ear transfer functions from the sound at the entrance of a blocked ear canal (or from the input of a headphone) to the sound at the eardrum for different listeners and headphones is developed based on an acoustic signal model of external ears. The model allows for applying realistic data about individual external ears and headphones and is advantageous over current standard ear simulators with fixed structures limited to simulating average ear canals and eardrum impedances below 10 kHz. Given different eardrum impedances, ear canal shapes, lengths, and headphones, the frequency responses of external-ear transfer functions are estimated and presented. In addition, a method of determining the Norton equivalent volume velocity or Thevenien equivalent sound pressure sources of a headphone from sound pressure signals in an acoustic tube is presented. These methods are validated via direct measurements and expected to have applications in headphone sound reproduction, headphone and hearing aid design, and audiometric and psychoacoustic measurements to produce desired sounds at the eardrums of different listeners. © *2015 Acoustical Society of America*. [http://dx.doi.org/10.1121/1.4926560]

[MRB] Pages: 694–707

I. INTRODUCTION

The acoustic transfer functions of external ears with or without headphones affect the features of perceived sounds such as loudness, timbre, speech intelligibility, and sound localization. In many applications, it is desired to know the effects of the transfer functions of external ears with or without headphones on perceived sounds. The sound transmission characteristics within and to external ears have been experimentally measured on normal human ears (Mehrgardt and Mellertl, 1977; Harmmershøi and Møller, 1996). The transfer functions from headphone inputs to eardrum sound pressure signals have been measured on 40 human ears for 14 headphones (Møller *et al.*, 1995). A method of estimating the sound pressure magnitude at the eardrum from pressure-velocity measurements at the entrance of the ear canal is developed assuming that no energy is absorbed by ear canals and eardrums (Hiipakka *et al.*, 2012). Although direct measurements help understand sound transmission within ear canals, measuring on human ears with or without headphones is not always convenient. A standard ear simulator might be used to measure the transfer function from the sound pressure at the entrance of the ear canal to the sound pressure at the eardrum or the transfer function from the input of a headphone to the sound pressure at the eardrum. Unfortunately, however, current standard ear simulators can only simulate average human eardrum impedance below 8–10 kHz (IEC, 2010), and hence they are inadequate for some applications. Moreover, they have fixed ear canals and eardrum impedance simulators and cannot simulate the effects caused by individual differences in ear canal and eardrum impedance.

To simulate the acoustic transfer functions of various external ears based on realistic models, there have been different approaches. A boundary element method is developed to calculate the sound response at the eardrum to sound waves of varying frequencies and angles given detailed three-dimensional information about the shapes and dimensions of a head and an external ear (Walsh *et al.*, 2004). Their calculation results show that the ear canal does not affect the directionality of sound waves to the eardrum and hence can be simplified as a cylindrical tube. Although the method can produce results approximate to direct measurements on human ears, external ears can in fact be represented using acoustic parameters to be computationally more efficient. A lumped-element model of ear canals with earphones is developed to estimate ear-canal sound pressures generated by earphones for normal and pathological ears, but the lumped-element ear canal model is only valid up to 4 kHz (Voss *et al.*, 2000). In estimating the sound transfer function from a headphone to the eardrum, the ear canal is modeled as a multi-sectional tube with the varying cross-sectional area function of an average human ear canal, and the eardrum impedance value measured with sound wave fronts completely different from those found in natural hearing conditions is used (Hudde *et al.*, 1999; Hudde and Engle, 1998a). It is noted that the simulation of acoustic transfer functions of human external ears must also take into account sound distributions in ear canals. An ear-canal replica with an eardrum impedance simulator being connected at the umbo position (the position of the eardrum center) is created, and the eardrum simulator is tuned to meet both the target

[a]Electronic mail: huid@ieee.org

 0001-4966/2015/138(2)/694/14/$30.00

effective eardrum impedance below 4 kHz and the standing wave ratios in human ears from 4 to 10 kHz (Stinson and Daigle, 2010). To overcome the limitations of ear simulators with fixed structures and meet the needs of digital audio signal processing, a discrete-time digital filter is constructed to simulate the sound transfer functions of different external ears based on an acoustic model, in which an ear canal is modeled as a multi-sectional loss-less tube with a varying cross-sectional area, a pinna reflection coefficient is approximated as a low-pass filter, and an eardrum reflection coefficient is approximated as a constant number (Deng and Yang, 2014).

When listening through a headphone, the external ear is coupled with a sound source and an acoustic load from the headphone, and the headphone-to-eardrum transfer function varies with listeners and headphones. A headphone is defined as a free air equivalent coupling (FEC) headphone if its acoustic load to the ear canal equals to the radiation impedance of a free pinna. If an FEC headphone is used to play back binaural sound signals received at the entrances of blocked ear canals and if the transfer function from the headphone input to the sound pressure at the entrance of a blocked ear canal is equalized for, then the correct eardrum sounds, which the listener would hear in the original sound field, can be reproduced approximately at his/her eardrums during the play back (Møller *et al.*, 1995; Hammershøi and Møller, 1996). However, ideal FEC headphones are hard to obtain. Even the acoustic loads of STAX SR l Professional open headphones to ears are not equal to the pinna radiation impedance (Voländer, 2000). For headphones to reproduce correct sounds at the eardrums, it is needed to estimate the eardrum sound signals and the headphone-to-eardrum transfer functions for various external ears.

The present research develops a method of estimating the frequency responses of external-ear transfer functions from the sound at the entrance of a blocked ear canal (or from the input of a headphone) to the sound at the eardrum based on an acoustic signal model. The model can accommodate measured data about individual external ears and headphones. Different from previous approaches, the ear canal is modeled as a chain of time delays, tube attenuations, and reflection coefficients. This approach allows for obtaining the transfer function in the discrete-time domain from the formulated frequency response. In Sec. II, the acoustic signal mode of external ears is presented. In Sec. III, the frequency response of an external-ear transfer functions is formulated in terms of ear canal reflection coefficients, eardrum impedance and reflection coefficient, pinna reflection coefficient or headphone reflection coefficient, and equivalent sound source. In Sec. IV, the effects of external ears and headphones on the transfer functions are investigated. The method for determining headphone and pinna reflection coefficients is described in Sec. V. The method for determining headphone Norton or Thevenien equivalent sound sources is presented in Sec. VI. Validation of the estimation method is presented in Sec. VII, and conclusion is contained in Sec. VIII.

II. THE ACOUSTIC MODEL

In this research, an ear canal is modeled as a one-dimensional tube with varying cross-sectional area function. This is based on the finding that an ear canal can be modeled using a straight one-dimensional tube with a varying cross-sectional area function up to 15 kHz with spatial variations of sound pressure level within each cross section being 1.5 dB at 8 kHz and 4.5 dB at 15 kHz (Stinson and Daile, 2005). The effect of an eardrum on sound transmission in the ear canal is modeled as an effective impedance Z_{TM} concentrated at the center (umbo) of the eardrum as in (Hudde and Engel, 1998a; Stinson, 1985; Stinson and Daigle, 2010). The umbo point is at a distance about 4 mm from the end of the ear canal for average ears. In this work, the portion of an ear canal from its entrance to the umbo is modeled using an M-sectional tube with each section having the same length L and a different cross-sectional area, and the residual ear canal is modeled using a four-sectional tube with sectional length $L_2 = 1$ mm, as shown in Fig. 1. The mth cross-sectional area of the ear canal model is denoted as S_m, $m = 1, 2,\ldots, M+4$. A sound source to an ear canal can be modeled using its Thevenien equivalent sound pressure source $p_0(t)$, which is the sound pressure at the entrance of the blocked ear canal, and a source acoustic impedance $Z_0(f)$ observed from the entrance of the ear canal into the space. Let the Fourier transform of $p_0(t)$ be $P_0(f)$, then the Norton equivalent volume velocity source $u_0(t)$ of the sound source is related to the Thevenien equivalent sound pressure source

$$U_0(f) = P_0(f)/Z_0(f), \tag{1}$$

where $U_0(f)$ is the Fourier transform of $u_0(t)$.

Sound waves in the ear canal can be represented using going-in and going-out volume velocities $u_m^+(t)$ and $u_m^-(t)$ at the beginning of the mth section, respectively, $m = 1,\ldots, M$, as shown in Fig. 1, where the beginning of the first section corresponds to the entrance of the ear canal. The acoustic impedance looking from the beginning of the $(M+i)$th section toward its end can be calculated according to the input impedance of a tube (Kinsler *et al.*, 2000)

$$Z_{M+i} = \frac{\rho c}{S_{M+i}} \frac{Z_{M+i+1} + j\frac{\rho c}{S_{M+i}} \tan(k_{M+i} L_2)}{\frac{\rho c}{S_{M+i}} + jZ_{M+i+1} \tan(k_{M+i} L_2)}, \tag{2}$$

where $i = 1,\ldots, 4$, Z_{M+5} is the acoustic impedance at the end of the ear canal, ρ is the air density, c is the sound speed in the ear canal, and k_m is the wave number of the sound in mth section. In general, if tube attenuation is considered, the

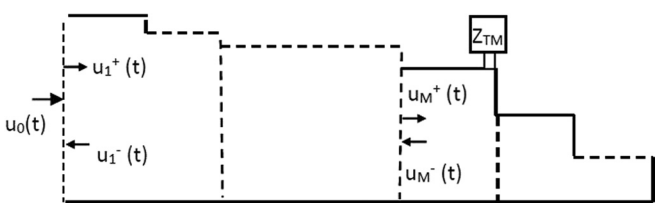

FIG. 1. The tube model of the ear canal.

wave number in the mth section can be determined as (ISO, 1998)

$$k_m = 2\pi f/c - j0.0194\sqrt{f}/D_m c, \tag{3a}$$

where D_m is the diameter of the mth section, and f is the frequency of the sound. It is found that the damping factor of human ear canals is about three times that of smooth brass tube (Hudde and Engel, 1998b). Thus in estimating sound transmission within ear canals, the following wave number is used:

$$k_m = 2\pi f/c - j0.0582\sqrt{f}/D_m c. \tag{3b}$$

The total acoustic impedance terminating the end of the Mth section is the parallel of Z_{TM} and Z_{M+1},

$$Z_T = Z_{TM} Z_{M+1}/(Z_{TM} + Z_{M+1}). \tag{4}$$

Given a sound field, let the Fourier transform of the sound pressure at the center of the eardrum be $P_{TM}(f)$, the Fourier transform of the volume velocity at the end of the Mth section of the tube model be $U_T(f)$. The relationship between $P_{TM}(f)$ and $U_0(f)$ or $P_0(f)$ can be derived from the tube model shown in Fig. 1 and the electro-acoustic analogue circuit model shown in Fig. 2 as follows.

III. ACOUSTIC TRANSFER FUNCTIONS OF EXTERNAL EARS

In this section, the frequency responses of the transfer functions from the sound signal at the entrance of a blocked ear canal or from the input of a headphone to the sound signal at the eardrum are formulated. The corresponding discrete-time signal transfer functions in the Z domain are also presented.

A. Transfer function from the entrance of the blocked ear canal to the eardrum

The frequency response of the transfer function from $P_0(f)$ to $P_{TM}(f)$ is

$$H_{0T}(f) \triangleq \frac{P_{TM}(f)}{P_0(f)} = \frac{Z_T(f)U_T(f)}{Z_0(f)U_0(f)}. \tag{5}$$

To obtain $H_{0T}(f)$, the frequency response of the transfer function from $U_0(f)$ to $U_T(f)$ needs to be derived. Let the going-in and going-out volume velocities of a sound signal with frequency f at the beginning of the mth section of the tube model be $U_m^+(f)$ and $U_m^-(f)$, respectively, $m = 1,\ldots, M$. Then

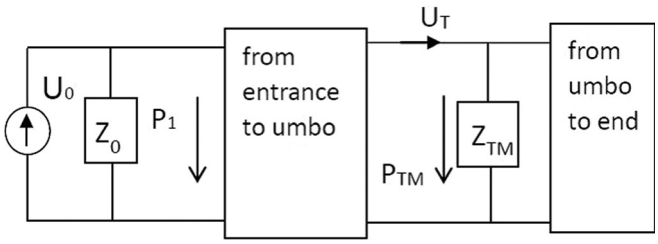

FIG. 2. The acoustic system of the external ear.

for planar sound waves in the tube, the going-in and going-out volume velocities at the end of the mth section can be derived as $U_m^+(f)\, e^{-jk_m L}$ and $U_m^-(f)\, e^{jk_m L}$, respectively (Kinsler *et al.*, 2000). At the boundary of the mth and $(m+1)$th sections, $m = 1,\ldots, M-1$, the continuity of volume velocity leads to the following equation:

$$U_m^+(f)e^{-jk_m L} + U_m^-(f)e^{jk_m L} = U_{m+1}^+(f) + U_{m+1}^-(f), \tag{6}$$

and the continuity of sound pressure leads to the following equation:

$$\begin{aligned}&(U_m^+(f)e^{-jk_m L} - U_m^-(f)e^{jk_m L})\rho c/S_m \\ &\quad = (U_{m+1}^+(f) - U_{m+1}^-(f))\rho c/S_{m+1}.\end{aligned} \tag{7}$$

Define the reflection coefficient at the left side of the boundary of the mth and $(m+1)$th sections as

$$r_m = (S_{m+1} - S_m)/(S_{m+1} + S_m). \tag{8}$$

Equations (6)–(8) lead to

$$U_{m+1}^+(f) = (1 + r_m)U_m^+(f)e^{-jk_m L} - r_m U_{m+1}^-(f), \tag{9}$$

and

$$U_m^-(f)e^{jk_m L} = r_m U_m^+(f)e^{-jk_m L} + (1 - r_m)U_{m+1}^-(f). \tag{10}$$

Equations (9) and (10) can be re-written as

$$\begin{bmatrix} U_m^+(f) \\ U_m^-(f) \end{bmatrix} = \frac{e^{jk_m L}}{1 + r_m} \begin{bmatrix} 1 & r_m \\ r_m e^{-jk_m 2L} & e^{-jk_m 2L} \end{bmatrix} \begin{bmatrix} U_{m+1}^+(f) \\ U_{m+1}^-(f) \end{bmatrix}. \tag{11}$$

At the end of Mth section, the continuity of sound pressure leads to

$$(U_M^+(f)e^{-jk_M L} - U_M^-(f)e^{jk_M L})\rho c/S_M = U_T(f)Z_T(f), \tag{12}$$

and the continuity of volume velocity leads to

$$U_M^+(f)e^{-jk_M L} + U_M^-(f)e^{jk_M L} = U_T(f). \tag{13}$$

Define the reflection coefficient at the end of the Mth section as

$$r_T(f) = (\rho c/S_M - Z_T(f))/(\rho c/S_M + Z_T(f)). \tag{14}$$

Equations (12)–(14) lead to

$$U_T(f) = (1 + r_T(f))U_M^+(f)e^{-jk_M L}, \tag{15}$$

and

$$U_M^-(f)e^{jk_M L} = r_T(f)U_M^+(f)e^{-jk_M L}. \tag{16}$$

Equations (15) and (16) can be re-written as

$$\begin{bmatrix} U_M^+(f) \\ U_M^-(f) \end{bmatrix} = \frac{e^{jk_M L}}{1 + r_T(f)} \begin{bmatrix} 1 \\ r_T(f)e^{-jk_M 2L} \end{bmatrix} U_T(f). \tag{17}$$

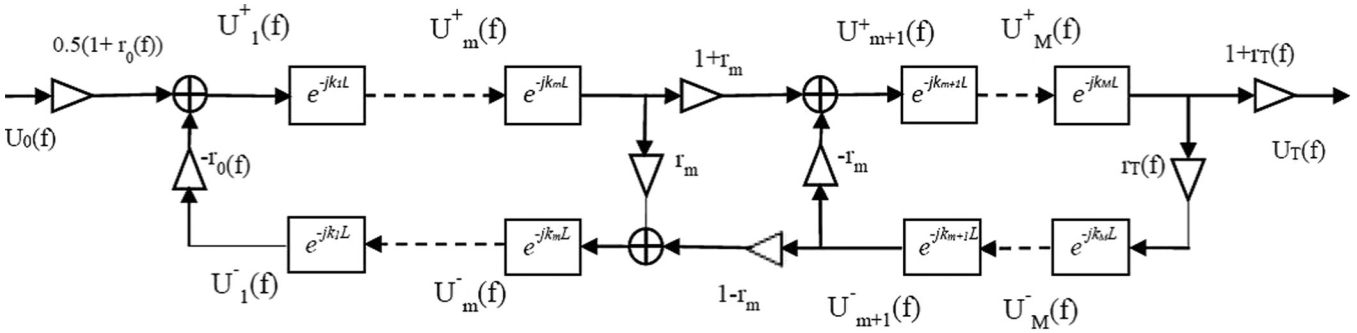

FIG. 3. The signal flow diagram of the volume velocities in the M-sectional tube model.

At the beginning of the first tube section, the continuity of sound pressure and of volume velocity leads to the following equation:

$$\begin{aligned} U_1^+(f) + U_1^-(f) &= U_0(f) - P_1(f)/Z_0(f) \\ &= U_0(f) - (U_1^+(f) - U_1^-(f))\rho c/Z_0(f)S_1. \end{aligned} \tag{18}$$

Define the reflection coefficient from the entrance of the ear canal as

$$r_0(f) = (Z_0(f) - \rho c/S_1)/(Z_0(f) + \rho c/S_1). \tag{19}$$

Then Eqs. (18) and (19) lead to

$$U_1^+(f) = 0.5(1 + r_0(f))U_0(f) - r_0 U_1^-(f), \tag{20}$$

and

$$U_0(f) = \frac{2}{1 + r_0(f)} \begin{bmatrix} 1 & r_0(f) \end{bmatrix} \begin{bmatrix} U_1^+(f) \\ U_1^+(f) \end{bmatrix}. \tag{21}$$

The relations between volume velocity signals in each section given by Eqs. (9), (10), (15), (16), and (20) can be summarized using the signal flow diagram shown in Fig. 3. This signal diagram has applications in modeling acoustic signal transmission in a tube as shown in Sec. VI and modeling speech sound production from a vocal tract. This signal diagram takes into account of the sound attenuation in each section; this is not considered in the tube model of a vocal tract (Deng *et al.*, 2006; Rabiner and Schafer, 2011).

Equations (11), (17), and (21) yield the frequency response of the transfer function from $U_0(f)$ to $U_T(f)$,

$$\frac{U_T(f)}{U_0(f)} = \frac{e^{-jk_M L} 0.5(1 + r_0(f))(1 + r_T(f)) \prod_{m=1}^{M-1} e^{-jk_m L}(1 + r_m)}{\begin{bmatrix} 1 & r_0(f) \end{bmatrix} \left\{ \prod_{m=1}^{M-1} \begin{bmatrix} 1 & r_m \\ r_m e^{-jk_m 2L} & e^{-jk_m 2L} \end{bmatrix} \right\} \begin{bmatrix} 1 \\ r_T(f) e^{-jk_M 2L} \end{bmatrix}}. \tag{22}$$

Substituting Eq. (22) to Eq. (5) yields the frequency response

$$\frac{P_{TM}(f)}{P_0(f)} = \frac{Z_T(f)}{Z_0(f)} \frac{e^{-jk_M L} 0.5(1 + r_0(f))(1 + r_T(f)) \prod_{m=1}^{M-1} e^{-jk_m L}(1 + r_m)}{[1, r_0(f)] \left\{ \prod_{m=1}^{M-1} \begin{bmatrix} 1 & r_m \\ r_m e^{-jk_m 2L} & e^{-jk_m 2L} \end{bmatrix} \right\} \begin{bmatrix} 1 \\ r_T(f) e^{-jk_M 2L} \end{bmatrix}}. \tag{23}$$

From Eq. (19), $Z_0(f)$ can be expressed in term of $r_0(f)$ as

$$Z_0(f) = \frac{\rho c}{S_1} \frac{1 + r_0(f)}{1 - r_0(f)}. \tag{24}$$

Substituting $Z_0(f)$ into Eq. (23) leads to

$$\frac{P_{TM}(f)}{P_0(f)} = \frac{Z_T(f)}{\rho c/S_1} \frac{e^{-jk_M L} 0.5(1 - r_0(f))(1 + r_T(f)) \prod_{m=1}^{M-1} e^{-jk_m L}(1 + r_m)}{[1, r_0(f)] \left\{ \prod_{m=1}^{M-1} \begin{bmatrix} 1 & r_m \\ r_m e^{-jk_m 2L} & e^{-jk_m 2L} \end{bmatrix} \right\} \begin{bmatrix} 1 \\ r_T(f) e^{-jk_M 2L} \end{bmatrix}}. \tag{25}$$

Given the preceding frequency response, the transfer function from $p_0(t)$ to $p_{TM}(t)$ can be determined; this is needed in some applications such as estimating binaural signals received at the centers of the eardrums in the sound field given binaural signals recorded at the entrances of blocked ear canals. It is noted that if tube attenuation can be ignored (i.e., $k_m = 2\pi f/c = k$) and if the sound signal is sampled at a sampling rate F_s that satisfies the following condition:

$$F_s = c/2L, \tag{26}$$

then $e^{-jk2L} = e^{-j2\pi f/Fs}$, and the discrete-time transfer function in the Z domain corresponding to the frequency response Eq. (25) can be formulated as

$$H_{0T}(z) = \frac{Z_T(z)}{\rho c/S_1} \frac{z^{-M/2} 0.5(1-r_0(z))(1+r_T(z)) \prod_{m=1}^{M-1}(1+r_m)}{[1, r_0(z)] \left\{ \prod_{m=1}^{M-1} \begin{bmatrix} 1 & r_m \\ r_m z^{-1} & z^{-1} \end{bmatrix} \right\} \begin{bmatrix} 1 \\ r_T(z) z^{-1} \end{bmatrix}}, \tag{27}$$

where $r_0(z)$, $r_T(z)$, and $Z_T(z)$ are the discrete-time transfer functions in the Z domain corresponding to the frequency responses $r_0(f)$, $r_T(f)$ and $Z_T(f)$, respectively.

B. Transfer function from the headphone input to the eardrum

It is noted that the model shown in Fig. 2 can also be used to model an ear canal coupled with a headphone, where U_0 is the Norton equivalent volume velocity source generated by the headphone to the ear canal entrance, and Z_0 is Z_{0ph}, the acoustic impedance looking from the entrance of the ear canal to the headphone. Let the headphone be excited by an electrical impulse signal and $U_{0ph}(f)$ be the Fourier transform of the Norton equivalent volume velocity source of the headphone in response to the impulse input of the headphone. If the headphone is excited by an electrical signal, the Fourier transform of which is $V_{ph}(f)$, then the Fourier transform of the Norton volume velocity source of the headphone to the ear canal is $U_0(f) = V_{ph}(f) U_{0ph}(f)$. The frequency response of the transfer function from the input of the headphone to the sound pressure at the eardrum can be derived from Eq. (22) as

$$H_{ph2TM}(f) \triangleq \frac{P_{TM}(f)}{V_{ph}(f)} = U_{0ph}(f) Z_T(f) \frac{e^{-jk_M L} 0.5\left(1 + r_{ph}(f)\right)\left(1 + r_T(f)\right) \prod_{m=1}^{M-1} e^{-jk_m L}(1 + r_m)}{\left[1, r_{ph}(f)\right] \left\{ \prod_{m=1}^{M-1} \begin{bmatrix} 1 & r_m \\ r_m e^{-jk_m 2L} & e^{-jk_m 2L} \end{bmatrix} \right\} \begin{bmatrix} 1 \\ r_T(f) e^{-jk_M 2L} \end{bmatrix}}, \tag{28}$$

where $r_{ph}(f)$ is determined via Eq. (19) by replacing $Z_0(f)$ with $Z_{0ph}(f)$. It is noted that $r_{ph}(f)$ and $U_{0ph}(f)$ are headphone-dependent and need to be measured.

Similarly, if the attenuation of the M-sectional tube can be ignored, and the sound signal is sampled at $F_s = c/2L$, then the discrete-time transfer function in the Z domain corresponding to the frequency response of Eq. (28) is

$$H_{ph2TM}(z) = U_{0ph}(z) Z_T(z) \frac{z^{-M/2} 0.5\left(1 + r_{ph}(z)\right)\left(1 + r_T(z)\right) \prod_{m=1}^{M-1}(1 + r_m)}{\left[1, r_{ph}(z)\right] \left\{ \prod_{m=1}^{M-1} \begin{bmatrix} 1 & r_m \\ r_m z^{-1} & z^{-1} \end{bmatrix} \right\} \begin{bmatrix} 1 \\ r_T(z) z^{-1} \end{bmatrix}}, \tag{29}$$

where $U_{0ph}(z)$ and $r_{ph}(z)$ are the discrete-time transfer functions corresponding to the frequency responses $U_{0ph}(f)$ and $r_{ph}(f)$, respectively.

IV. EFFECT OF EXTERNAL EARS AND HEADPHONES

The formulation of frequency responses of external-ear transfer functions makes it easy to investigate the effects of eardrum impedances, ear canal cross-sectional area functions, headphone reflection coefficients, and equivalent sound sources on the responses of the transfer functions. In this section, some examples of the affecting factors are presented. Then their effects on the frequency responses of the transfer functions are estimated.

A. Pinna reflection coefficient

Perceptually, pinna reflection coefficient contributes to the acoustic cues of natural spatial hearing not wearing headphones. Physically it affects the frequency spectra of the sound signals received at the eardrum. The pinna reflection coefficient can measured through an acoustic impedance tube. Detailed descriptions about the measurement method are presented in Sec. V. The measured magnitude and phase responses of the pinna reflection coefficient are shown in

Figs. 4(a) and 4(b), respectively. As frequency increases from zero to about 7 kHz, the pinna reflection coefficient magnitude monotonically decreases from 1 to about 0.4. At higher frequencies, the pinna reflection coefficient magnitude exhibits peaks and valleys due to the resonance of the concha. The result is similar to that in Hudde and Engel (1998b), which is measured on a replica of a real human pinna connected to an acoustic impedance tube positioned through the ear canals of an artificial head.

B. Eardrum impedance

Although various data about eardrum impedances have been published, only eardrum impedance data covering a wide frequency range are considered in this research to investigate the effect of eardrum impedance on the transfer functions. It is found that two eardrum impedances presented in Hudde and Engel (1998c) cover a wide frequency range from 160 Hz to 16 kHz. Therefore they are considered in this research. Their magnitude and phase frequency responses are plotted in Figs. 4(c) and 4(d) using solid lines (labeled as Z_{TM1}) and dotted lines (labeled as Z_{TM2}), respectively. It is noted that Z_{TM1} is measured "close to the eardrum" with sound wave fronts impinging on to the eardrum that make the eardrum vibrate in a condition not found in real hearing, and the value of Z_{TM1} is directly related to the middle ear impedance. In contrast, Z_{TM2} is developed from an effective eardrum impedance model in Shaw (1975) for ear simulators to meet both measured eardrum impedances at low frequencies and the measured standing wave ratios in real ears at high frequencies.

C. Ear canal area function

To estimate the effects of various ear canal area functions on external-ear transfer functions, the following four different ear canal area functions are chosen: (1) the model ear canal area function specified in Hudde and Engel (1998c) and Stinson and Lawton(1989), which is re-sampled to have 16 sections beginning from the entrance of the ear canal with the first 12 sections each being $L = 2$ mm long and the last 4 sections each being $L_2 = 1$ mm long, the umbo point being at 4 mm from the end of the ear canal, and each sectional area being the value of the area function of the model ear canal at the middle of the section, as shown using the solid line in Fig. 4(e); (2) and (3) short and long model ear canal area function with the same sectional areas as the model ear canal, but their first 12 sectional lengths being $L = 1.6$ mm and $L = 2.4$ mm, respectively, as shown using the dashed line and the dashed-dotted line, respectively, in Fig. 4(e); (4) a "uniform" ear canal area function with a constant cross-sectional area from the entrance of the ear canal to the umbo point that is equal to the area of the entrance of the model ear canal and with the same total length and the cross-sectional area from the umbo to the end as the model ear canal, as shown using the dotted line in Fig. 4(e). For the first three ear canal area functions, the reflection coefficients r_m ($m = 1, \ldots, 11$), r_0 and r_T are unchanged; while for the last ear canal area function, r_0 is unchanged, but $r_m = 0$ ($m = 1, \ldots, 11$), and r_T needs to be re-calculated according to Eq. (14) given that S_M equals to the area of the entrance of the model ear canal.

D. The effect of eardrum impedance

Given an eardrum impedance and the area function, the total acoustic impedance Z_T at the end of the Mth section can be derived according to Eqs. (2), (3b), and (4) assuming that Z_{M+5} at the end of the ear canal is infinite. Next the reflection coefficient r_T at the end of section M is determined according to Eq. (14). Now, given r_T, the model ear canal area function and the measured pinna reflection coefficient, the frequency response $P_{TM}(f)/P_0(f)$ is estimated according to Eq. (23). The frequency response $P_{TM}(f)/P_0(f)$ containing the effect of the eardrum impedance Z_{TM1} is shown using the solid line in Fig. 5, and the one containing the effect of Z_{TM2} is shown using the dotted line in Fig. 5. It shows that eardrum impedances mainly affect the resonance peaks and frequencies, and a larger eardrum impedance results in stronger

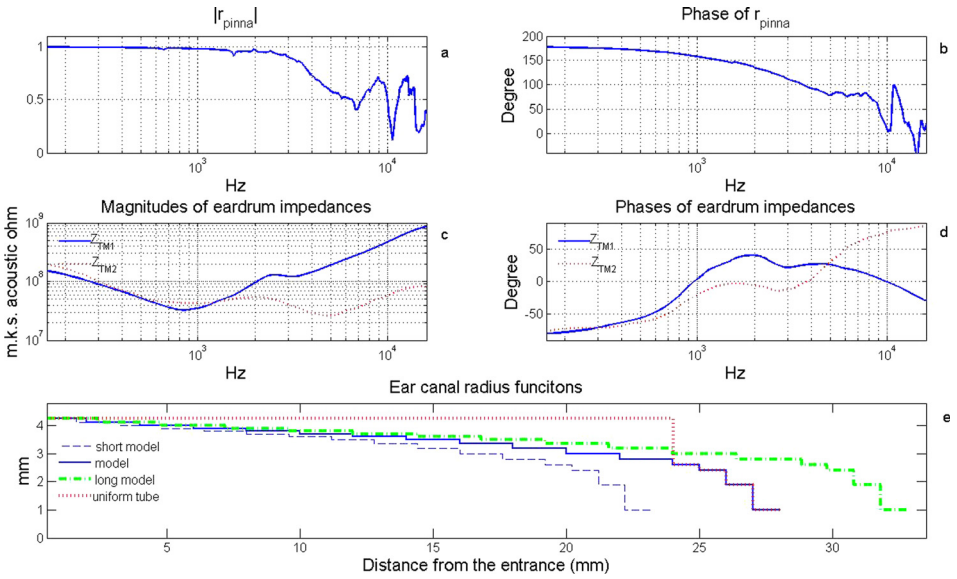

FIG. 4. (Color online) Examples of factors affecting external-ear transfer functions. (a) and (b) magnitude and phase frequency responses of a pinna reflection coefficient; (c) and (d) magnitude and phase frequency responses of two eardrum impedances (Hudde and Engel, 1998c); (e) ear canal radius functions: model ear canal radius function with the first 12 sectional lengths being $L = 2$ mm (solid line); short and long model ear canals with the first 12 sectional lengths being $L = 1.6$ mm (dashed line) and $L = 2.4$ mm (dashed-dotted line), respectively; constant ear canal from the entrance of the ear canal to the umbo with the same length and residual ear canal as the model ear canal (dotted line).

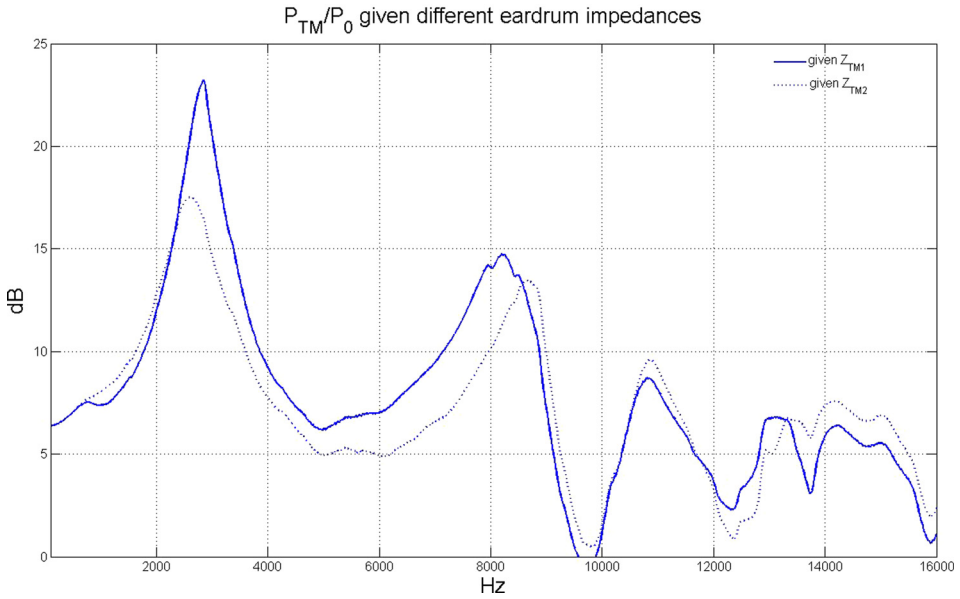

FIG. 5. (Color online) The frequency responses of the sound pressure transfer functions from the entrance of a blocked ear canal to the eardrum center estimated given eardrum impedance Z_{TM1} (solid line) and Z_{TM2} (dotted line), respectively.

resonance peaks. It is noted that Z_{TM1} is measured in a condition different from a natural hearing condition, and that Z_{TM2} is more relevant to sound transmission in ear canals in natural hearing condition than Z_{TM1} does as mentioned in Sec. IV B. Thus Z_{TM2} is chosen in the following estimations of external-ear transfer functions.

E. The effect of ear canal area function

Given the measured pinna reflection coefficient and $r_T(f)$ determined from the eardrum impedance $Z_{TM2}(f)$, $P_{TM}(f)/P_0(f)$ is estimated according to Eq. (23) for the four specified ear canals, respectively. The results corresponding to the four ear canals are shown using solid line, dashed line, dashed-dotted line, and dotted line in Fig. 6, respectively. For the first three ear canals with the same sectional areas but different sectional lengths, as the length of the ear canal increases, the resonance frequencies of $P_{TM}(f)/P_0(f)$ decrease. Comparing the frequency response of the model ear canal (solid line in Fig. 6) with that of the "uniform" ear canal (dotted line in Fig. 6), it can be seen that the first and second resonance frequencies of the model ear canal are larger than the corresponding ones of the "uniform" ear canal, although the two ear canals have the same total length. This can be explained by the finding that one effect of a varying cross-sectional area of an ear canal is to compress and stretch out the standing wave patterns in the ear canal (Stinson, 1990).

F. The effects of headphones

The reflection coefficient and the Norton equivalent volume velocity source of a headphone to the ear canal can be measured using the methods described in Secs. V and VI, respectively. In this work, the left piece of a Sennheiser IE 60 insert headphone and the left piece of a Sennheiser HD 598 circumaural open headphone are measured. For the IE 60 insert headphone, the measured magnitude and phase

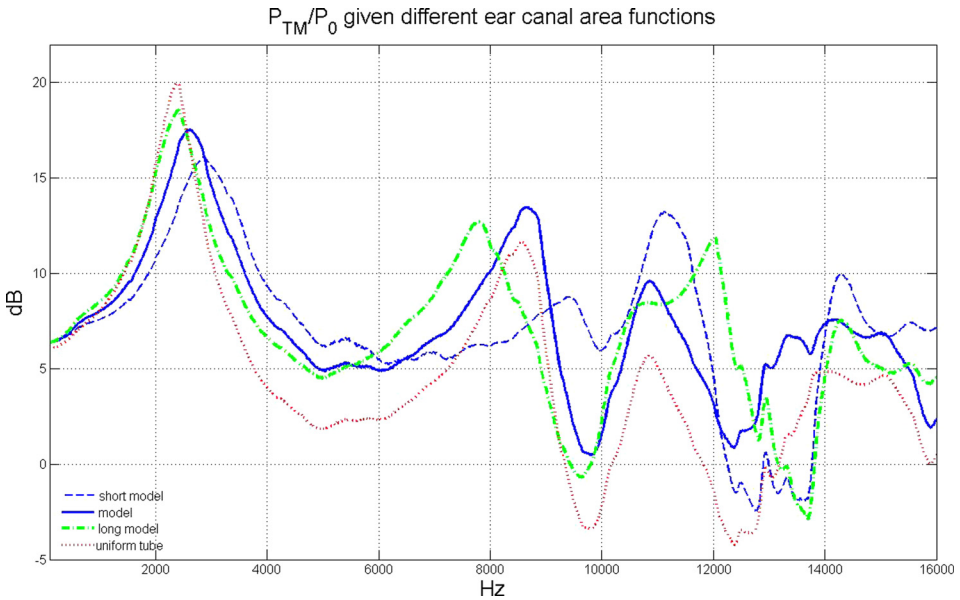

FIG. 6. (Color online) The frequency responses of the sound transfer function from the entrance of a blocked ear canal to the eardrum center estimated given different ear canal area functions, respectively.

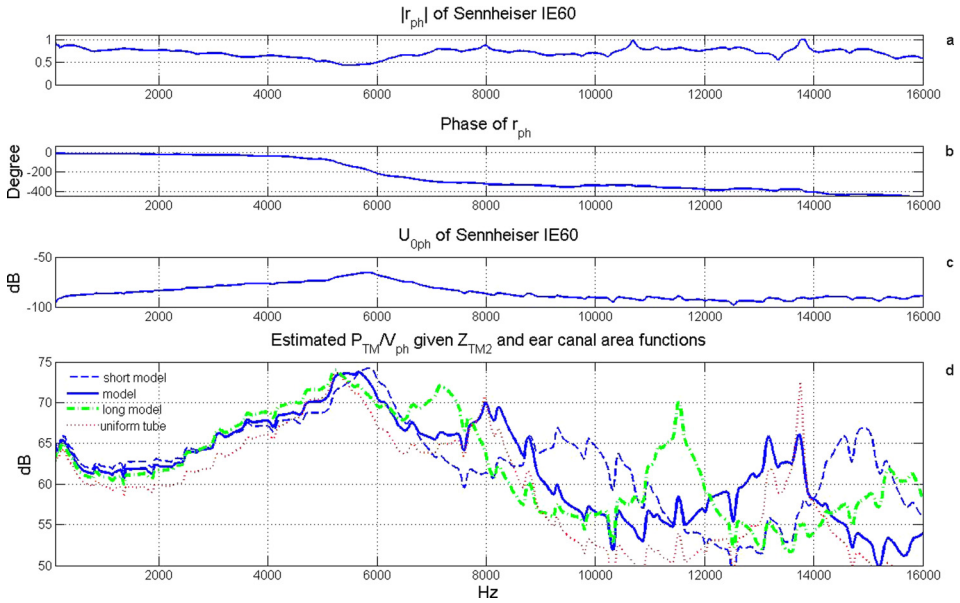

FIG. 7. (Color online) (a) The magnitude frequency response of the reflection coefficient of the Sennheiser IE 60 insert headphone; (b) the phase frequency response of the reflection coefficient of the headphone; (c) the frequency response of the Norton equivalent volume velocity source of the headphone; (d) the frequency responses of the headphone-to-eardrum sound pressure transfer function estimated for the ear canal area functions defined in Fig. 4(e).

frequency responses of the reflection coefficient r_{ph} and the magnitude frequency response of the Norton equivalent volume velocity source U_{0ph} are plotted in Figs. 7(a), 7(b) and 7(c), respectively. Given $r_{ph}(f)$, $U_{0ph}(f)$, and the eardrum impedance $Z_{TM2}(f)$, the frequency response $P_{TM}(f)/V_{ph}(f)$ of the IE 60 is estimated according to Eq. (28) for the four ear canal area functions, respectively. The results corresponding to the four ear canals are plotted in Fig. 7(d) using solid line, dashed line, dashed-dotted line, and dotted line, respectively. It is observed that for the IE 60 insert headphone, the first resonance frequency (5–6 kHz) of each $P_{TM}(f)/V_{ph}(f)$ is much higher than that (2–3 kHz) of the $P_{TM}(f)/P_0(f)$ corresponding to the same ear canal. This is caused by the large phase difference between r_{ph} (the headphone reflection coefficient) and r_{pinna} (pinna reflection coefficient) as can be seen from Figs. 4(b) and 7(b).

Similarly, for the Sennheiser HD 598 headphone, the measured magnitude and phase frequency responses of its reflection coefficient and the magnitude frequency response of its Norton equivalent volume velocity source are shown in Figs. 8(a), 8(b), and 8(c), respectively. Given $r_{ph}(f)$, $U_{0ph}(f)$ and eardrum impedance $Z_{TM2}(f)$, $P_{TM}(f)/V_{ph}(f)$ is estimated for the four ear canal area functions, respectively. The results are plotted using solid line, dashed line, dashed-dotted line, and dotted line in Fig. 8(d), respectively. It is shown that the first resonance frequency of each $P_{TM}(f)/V_{ph}(f)$ is close to that of the $P_{TM}(f)P_0(f)$ corresponding to the same ear canal (Fig. 6). This is because of that the phase of this headphone reflection coefficient below 4 kHz is close to that of the pinna reflection coefficient, which can be seen by comparing Fig. 8(b) with Fig. 4(b). It is also shown that each $P_{TM}(f)/V_{ph}(f)$ exhibits a sharp fall near 9.1 kHz. This is caused by the drop in the Norton equivalent volume velocity source near that frequency [Fig. 8(c)] due to the reflections between the headphone inner surface and the pinna, not dependent on the ear canal.

Comparing the estimated $P_{TM}(f)/V_{ph}(f)$ of HD 598 [Fig. 8(d)] with those of IE 60 [Fig. 7(d)], one can see that above

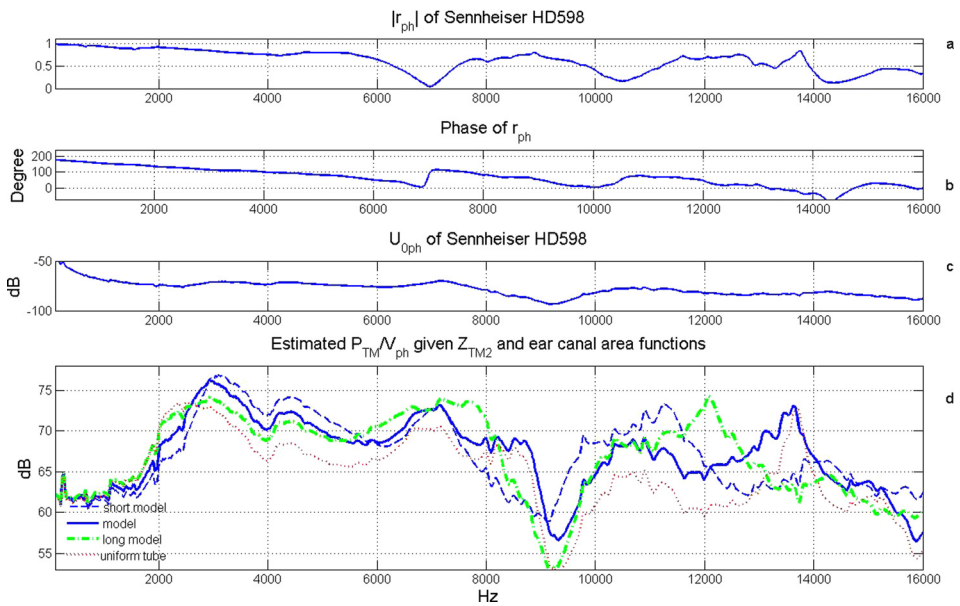

FIG. 8. (Color online) (a) The magnitude frequency response of the reflection coefficient of the Sennheiser HD 598 headphone; (b) the phase frequency response of the reflection coefficient of the headphone; (c) the frequency response of the Norton equivalent volume velocity source of the headphone; (d) the frequency responses of the headphone-to-eardrum transfer function estimated for the ear canal area functions defined in Fig. 4(e).

6 kHz, the difference in the magnitude resonance caused by the difference in ear canal length and shape is generally less for HD 598 than for IE 60. This can be explained by that the reflection coefficient magnitude of HD 598 is smaller than that of IE 60 at most frequencies above 6 kHz. For both IE 60 and HD 598 headphones, their $P_{TM}(f)/V_{ph}(f)$ frequency responses are low at low frequencies. The estimated frequency responses of the headphone-to-eardrum transfer functions are validated in Sec. VII.

V. DETERMINATION OF PINNA AND HEADPHONE REFLECTION COEFFICIENTS

It can be shown that the pinna or headphone reflection coefficient determined by Eq. (19) equals to the sound pressure reflection coefficient of the pinna or headphone acoustic impedance observed from the ear canal entrance. In this section, the measurement equipment and method for determining the pinna and headphone reflection coefficients used in Sec. IV are described.

A. Equipment

In this research, an acoustic impedance tube with a pinna simulator (AITP) is constructed for the measurements as illustrated in Fig. 9. The tube is made from a stainless steel tube with an inner diameter $D_0 = 8$ mm to simulate an average ear canal entrance diameter, an outer diameter 20 mm, and a length 380 mm. The cut-off frequency of plane waves in the tube is 0.58 c_0/D_0, where c_0 is the sound speed in the tube. One end of the tube is connected to a standard small left pinna simulator removed from a dummy head GRAS 45 BM. The other end of the tube is terminated with a sound source, an insert headphone (the right piece of the Sennheiser IE 60) to produce the excitation sounds to the tube to test the reflection coefficients at the simulated ear canal entrance. A circular plate with a diameter 150 mm and thickness 40 mm is used to connect the pinna simulator and the tube and also to simulate the cheek and head area around a pinna.

The reflection coefficient of the pinna or a headphone can be determined through the sound pressure signals in the AITP in response to the excitation sounds produced from the terminal sound source. According to the standard (ISO, 1998), the working frequency range of an impedance tube is determined by the distance s in meters between two

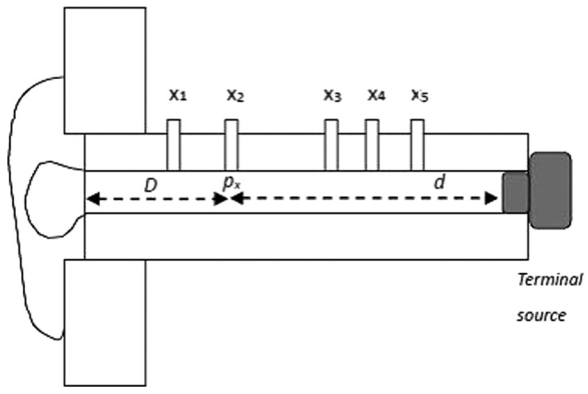

FIG. 9. The sketch of the acoustic impedance tube with pinna (AITP).

measurement positions in the tube, which is $0.05\ c_0/s < f < 0.45\ c_0/s$. In practice, increasing the number of measurement positions can improve the measurement accuracy (Boden and Abom, 1986). In the present work, five measurement positions are chosen: $x_1 = 52$ mm, $x_2 = 64.5$ mm, $x_3 = 129$ mm, $x_4 = 137$ mm, $x_5 = 162$ mm from the entrance of the ear canal of the pinna simulator. Combining the sound signals at all these positions can lead to final measured reflection coefficients over the frequency range $155\ \text{Hz} < f < 19\ \text{kHz}$, i.e., $0.05c_0/0.008 < f < 0.45c_0/0.11$. At these positions, five holes each with a diameter 4 mm and an axis perpendicular to the axis of the tube are made through the wall of the tube to insert measurement microphones. When measuring the reflection coefficient of a headphone, the headphone is silently coupled to the tube via the pinna simulator.

B. Method

To test pinna or headphone reflection coefficients to the entrance of an ear canal, the AITP should be excited from the terminal sound source. Let the Fourier transform of the planar sound pressure wave in the AITP incident to the entrance at $x = 0$ be $P_i(f)$ and that of the planar sound pressure wave in the AITP reflected from the entrance at $x = 0$ be $P_r(f)$. Then the Fourier transforms of sound pressure signals in the AITP at positions $x_1, x_2, \ldots, x_N$ can be expressed as

$$\begin{bmatrix} P_1(f) \\ P_2(f) \\ \vdots \\ P_N(f) \end{bmatrix} = \underbrace{\begin{bmatrix} e^{jkx_1} & e^{-jkx_1} \\ e^{jkx_2} & e^{-jkx_2} \\ \vdots & \vdots \\ e^{jkx_N} & e^{-jkx_N} \end{bmatrix}}_{A} \begin{bmatrix} P_i(f) \\ P_r(f) \end{bmatrix} = A \begin{bmatrix} P_i(f) \\ P_r(f) \end{bmatrix}, \quad (30)$$

and k is the complex wave number determined by the diameter of the tube shown in Eq. (3a). It is noted that the chosen measurement positions make A full rank over the frequency range $0 < f < 20$ kHz, and a solution of $P_i(f)$ and $P_r(f)$ can be obtained in the least square error sense from Eq. (30) via pseudo-inversion (Golub and Loan, 2013)

$$\begin{bmatrix} P_i(f) \\ P_r(f) \end{bmatrix} = \{A^T A\}^{-1} A^T \begin{bmatrix} P_1(f) \\ P_2(f) \\ \vdots \\ P_N(f) \end{bmatrix}. \quad (31)$$

Given the obtained $P_i(f)$ and $P_r(f)$, then the frequency response of the reflection coefficient of the pinna or a headphone can be determined

$$r_0(f) = P_r(f)/P_i(f). \quad (32)$$

In this research, the excitation signal for the measurements is an exponential sweep tone from 20 Hz to 20 kHz. The sound pressure signals at the five positions in the tube are measured in five sessions using a single miniature microphone Sonion 8002 with a diameter of 2.6 mm. When

measuring at one position, the microphone is inserted and sealed to the hole with its diaphragm flush with the interior surface of the AITP, and the other holes are sealed with metal columns and PTFE tapes. Appropriate playing and recording levels are set not to cause distortions and clipping to the recorded sound signals. The sound pressure at each position in response to the sweep tone is recorded simultaneously with the excitation signal via a B&K PULSE at a sampling rate $F_s = 65\,536$ Hz. The microphone recordings are filtered through a finite impulse response (FIR) low-pass filter with cut-off frequency $F_c = 20$ kHz to reduce high-frequency noise. At each measurement position x_i ($i = 1, \ldots, 5$), three impulse responses of the sound pressure are extracted from three recorded sweep tone responses, keeping their delays relative to the excitation impulses unchanged and hence making the relative delays between signals at two different positions recoverable. Each extracted impulse response is truncated to 0.05 s after and 300 samples before the excitation impulse. The averaged impulse response at each position x_j is taken to calculate the Fourier transform $P_j(f)$, $j = 1, \ldots, 5$, in Eq. (30). The pinna or a headphone reflection coefficient r_0 is then obtained from Eqs. (31) and (32). Because a single microphone is used in calculating the ratio of the reflected pressure to the incident pressure in Eq. (32), the frequency response of the microphone and that of the excitation sound source are not contained in the resulting r_0 (r_{pinna} or r_{ph}) and then Z_0 (Z_{pinna} or Z_{ph}) of the pinna or the headphone under test can be determined according to Eq. (24).

VI. DETERMINATION OF HEADPHONE EQUIVALENT SOUND SOURCES

It is known that the Norton or Thevenien equivalent sound sources of a headphone can be measured through known acoustic impedances and microphone signals (Hudde and Engel, 1996) or particle velocity sensor signals (Hiipakka, 2011). However, as shown in the following text, these equivalent sound sources of a headphone to the ear canal can be measured through sound pressure signals in the AITP in response to the excitation sound produced by the headphone under test without using additional acoustic impedance device or a particle velocity sensor.

A. Method

1. Step 1

Measure the reflection coefficient of the terminal sound source of the AITP by setting the terminal sound source to silence and producing the excitation sound from an insert headphone coupled to the ear canal entrance of the AITP. The reflection coefficient r_s of the terminal can be determined according to Eqs. (30)–(32), where the coordinates $x_1, \ldots, x_5$ should be the distances from the five microphone positions to the surface of the terminal source $d_1, \ldots, d_5$, respectively.

2. Step 2

Couple the headphone under test to the pinna simulator of the AITP and measure the reflection coefficient of the headphone. Keeping the connection between the terminal sound source and the AITP unchanged as in step 1 and produce the excitation sound from the terminal sound source of the AITP. The headphone reflection coefficient r_{ph} can be determined according to Eqs. (30)–(32) with coordinates of $x_1, \ldots, x_5$ being the distances from the five measurement position to the entrance of the ear canal of the AITP.

3. Step 3

Keeping the connection of the headphone under test to the AITP unchanged as in step 2, keeping the connection between the terminal sound source to the AITP unchanged as in steps 1 and 2 and setting the terminal sound source to be silent, play the excitation sound from the headphone under test and record the sound signal $p_x(t)$ in the AITP at a chosen position x.

4. Step 4

Determine the equivalent sound sources of the headphone as follows.

Assume the measured reflection coefficient of the terminal sound source of the AITP is r_s, then the terminal acoustic impedance of the AITP can be determined (ISO, 1998)

$$Z_{sa}(f) = \frac{\rho c}{S}(1 + r_s(f))/(1 - r_s(f)), \tag{33}$$

where S is the cross-sectional area of the AITP. The acoustic impedance looking from position x toward the terminal impedance Z_{sa} is (Kinsler *et al.*, 2000)

$$Z_{xsa} = \frac{\rho c}{s}\left(Z_{sa} + j\frac{\rho c}{s}\tan(kd)\right)\Big/\left(\frac{\rho c}{s} + jZ_{sa}\tan(kd)\right), \tag{34}$$

where d is the distance from position x to the surface of the terminal impedance as shown in Fig. 9.

Let the total volume velocity at position x in the AITP be U_x, and the Norton equivalent volume velocity source of the headphone under test to the entrance of the ear canal be U_{0ph}. Then the relationship between U_{0ph} and U_x can be modeled using the signal model shown in Fig. 10. This model is derived in a way similar to the approach for obtaining the ear canal transfer function model shown in Fig. 3 by modeling the section from the entrance of the AITP to the position x as one section with length D and a constant diameter along its length.

It is noted that similar to the definition of r_T in Eq. (14), r_{xs} in Fig. 10 is defined as

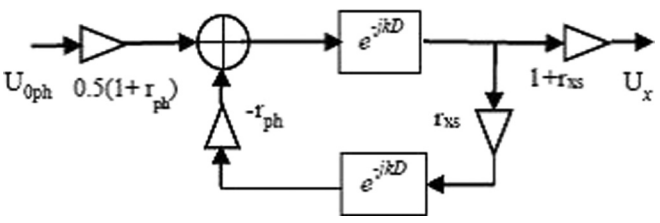

FIG. 10. The model of volume velocity signals in a tube.

$$r_{xs} = (\rho c/S - Z_{sxa})/(\rho c/S + Z_{sxa}) \quad (35)$$

and that $r_{xs} = -r_s e^{-j2kd}$.

In the frequency domain, the sound pressure signal at position x is related to U_{0ph} as

$$P_x = Z_{xsa} U_x = Z_{xsa} U_{0ph} \frac{0.5e^{-jkD}(1+r_{ph})(1+r_{xs})}{1+r_{ph}r_{xs}e^{-jk2D}}, \quad (36)$$

where P_x and U_x are the Fourier transforms of the sound pressure signal and the total volume velocity signal at the position x, respectively. Thus given P_x, r_{ph}, r_{xs}, Z_{xsa}, and D, the equivalent volume velocity source of the headphone can be derived from Eq. (36) as

$$U_{0ph} = \frac{P_x}{Z_{xsa}} \frac{1+r_{ph}r_{xs}e^{-2jkD}}{0.5e^{-jkD}(1+r_{ph})(1+r_{xs})}, \quad (37)$$

and the Thevenien equivalent pressure source of the headphone is

$$P_{0ph} = U_{0ph} Z_{0ph}, \quad (38)$$

where Z_{0ph} can be determined using Eq. (24) by substituting r_0 with r_{ph} and $S_1 = \pi(0.004)^2$. In this research, the Fourier transform of the sound pressure signal at position $x_2 = 64.5$ mm (from the entrance of the ear canal of the AITP) in response to the headphone excitation impulse signal is used as P_x in Eq. (37).

B. Experiment results

The magnitude and phase frequency responses of the terminal source reflection coefficient r_{sa} determined from step 1 are plotted using dotted lines in Figs. 11(a) and 11(b), respectively. The magnitude and phase frequency responses of the reflection coefficient of the left piece of the Sennheiser HD 598 headphone determined from step 2 are shown again using solid lines in Figs. 11(a) and 11(b) [same as in Figs. 8(a) and 8(b)]. The $P_x(f)$ of the Sennheiser HD 598 measured in step 3 is plotted in Fig. 11(c). The periodic ripples of $P_x(f)$ are caused by the periodic ripples of $Z_{sxa}(f)$ determined by d in Eq. (34) as shown using the dotted line in Fig. 11(d). The $U_{0ph}(f)$ obtained via Eq. (37) does not contain the periodic ripples as shown in Fig. 8(c) for Sennheiser HD 598. For comparison, the $U_{0ph}(f)$ obtained for the Sennheiser IE 60 insert headphone determined using this method can be seen in Fig. 7(c). The magnitude frequency response of Z_{0ph} of the Sennheiser HD 598 determined via Eq. (24) is shown using solid line in Fig. 11(d). The frequency responses of the Thevenien equivalent sound pressure source P_{0ph} of the Sennheiser HD598 headphone estimated according to Eq. (38) is plotted using the dotted line in Fig. 11(e).

To validate the method of determining the equivalent sound sources of a headphone, the Thevenien equivalent sound pressure source of the Sennheiser HD598 is directly measured at the entrance of the blocked ear canal of the AITP, as plotted using the solid line in Fig. 11(e). It can be seen that, the $P_{0ph}(f)$ estimated from the sound pressure signals in the AITP agrees well with the directly measured one. The difference is mainly caused by the difference in positioning the headphone before and after blocking the entrance of the ear canal simulator to estimate and measure P_{0ph}, respectively. It is noted that both the measured and estimated $P_{0ph}(f)$ exhibit a sharp fall near 9.1 kHz. This is explained by the reflections between the inner surface of the circum-aural headphone and the pinna.

It is noted that the Thevenien equivalent sound pressure source $P_{0ph}(f)$ is determined as the product of $Z_{0ph}(f)$ and $U_{0ph}(f)$ using Eq. (38) and that Z_{0ph} and U_{0ph} are determined independently. Therefore the good agreement between the $P_{0ph}(f)$ determined via the sound signals in the AITP and the directly measured one implies that the method of determining the reflection coefficients and the method of determining the Norton volume velocity and the Thevenien sound pressure sources of headphones are correct.

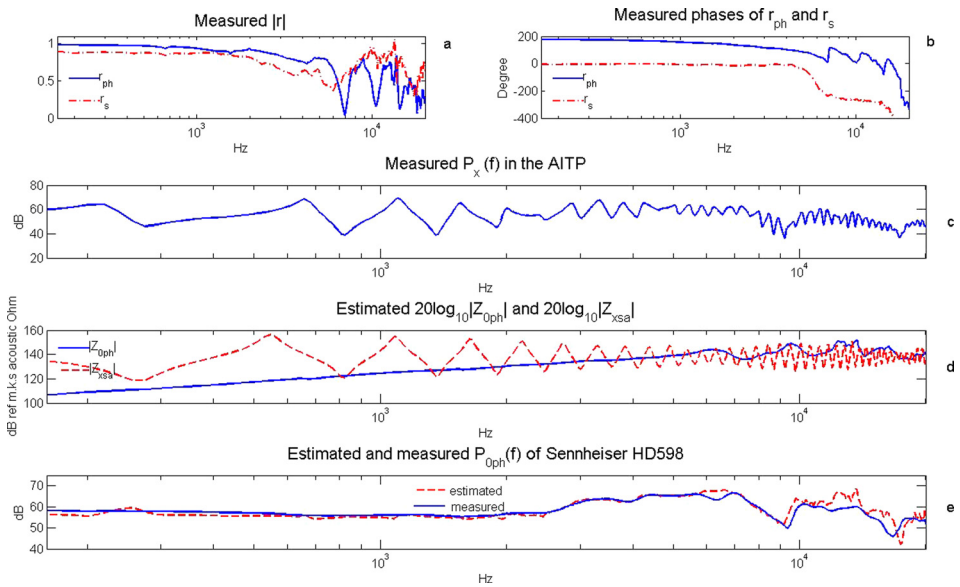

FIG. 11. (Color online) (a) The magnitude frequency responses of the reflection coefficient r_{ph} of Sehhneiser HD 598 headphone (solid line) and of the terminal reflection coefficient r_s (dashed-dotted line); (b) the phase frequency responses of r_{ph} (solid line) and of r_s (dashed-dotted line); (c) the measured $P_2(f)$; (d) the estimated $Z_{0ph}(f)$ (solid line) and $Z_{sxa}(f)$ (dashed line); (e) the estimated $P_0(f)$ (dashed line) and the measured P_{0ph} (solid line) for Sehhneiser HD 598.

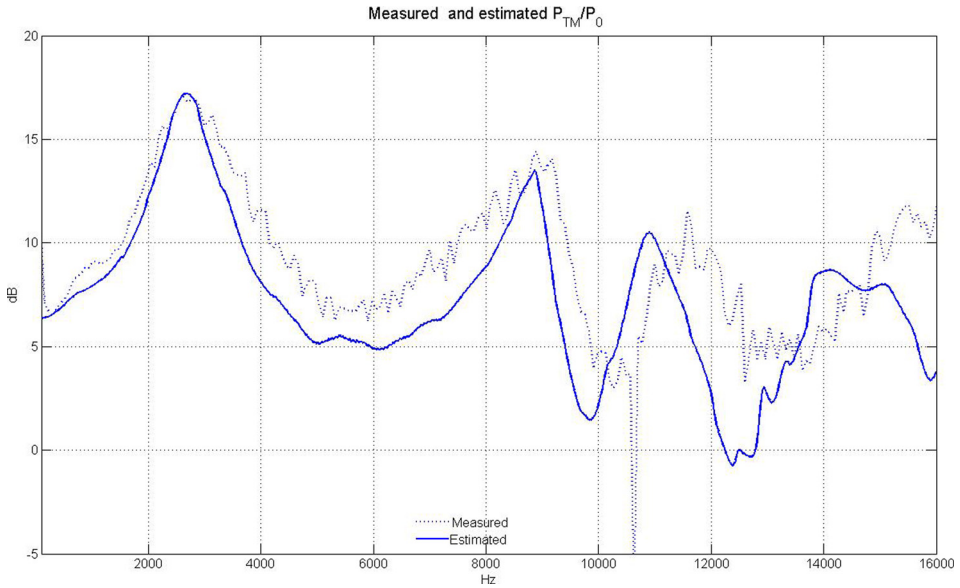

FIG. 12. (Color online) The frequency response of the sound pressure transfer function from the entrance of a blocked ear canal to the eardrum center measured on B&K HATS 4128 (dotted line), and the estimated one (solid line) given the model ear canal with the first 12 sectional lengths being $L = 1.9$ mm.

VII. VALIDATION OF THE ESTIMATION METHOD

Validating the estimated frequency responses of transfer functions of external ears through direct measurements on real human ears is difficult because of the difficulty in obtaining the eardrum impedances and ear canal area functions of real human ears. In this research, the estimation method is validated through direct measurements on standard ear simulators.

A. The transfer function from the entrance of a blocked ear canal to the eardrum

To validate the estimation method, the estimated $P_{TM}(f)/P_0(f)$ is compared to the one measured on a standard ear simulator in a dummy head. The measured $P_{TM}(f)/P_0(f)$ is obtained on a B&K dummy head HATS type 4128-C as shown using the dotted line in Fig. 12. The dummy head has two ear simulators compiling with IEC 60318-4 and two pinnae simulators compiling with ITU-T Rec. P.57 type 3.3. A full-band ball-shaped loudspeaker (with a diameter 11 cm and diaphragm diameter 8 cm) is positioned at 0.5 m from the dummy head right ear and produced an exponential sweep tone signal from 20 Hz to 20 kHz. $p_0(t)$ is measured at the entrance of the blocked right ear canal of the dummy head using the miniature microphone (Sonion 8002), which is inserted and aligned to the entrance of the ear canal, and the gap between the microphone and the ear canal is tightly filled with putty. Removing the miniature microphone and putty and keeping the positions of the dummy head and the loudspeaker unchanged, the same sweep signal is played back from the loudspeaker again and record $p_{TM}(t)$ at the eardrum of the ear simulator using the built-in microphone in the dummy head. $p_0(t)$ and $P_{TM}(t)$ are recorded using a B&K PULSE at a sampling rate $F_s = 65\,536$ Hz with 16 bits per sample, respectively. The impulse responses of the sound pressure signals at the eardrum of the ear simulator and at the entrance of blocked ear canal of the dummy head are extracted by convolving the recordings of $p_0(t)$ and $p_{TM}(t)$

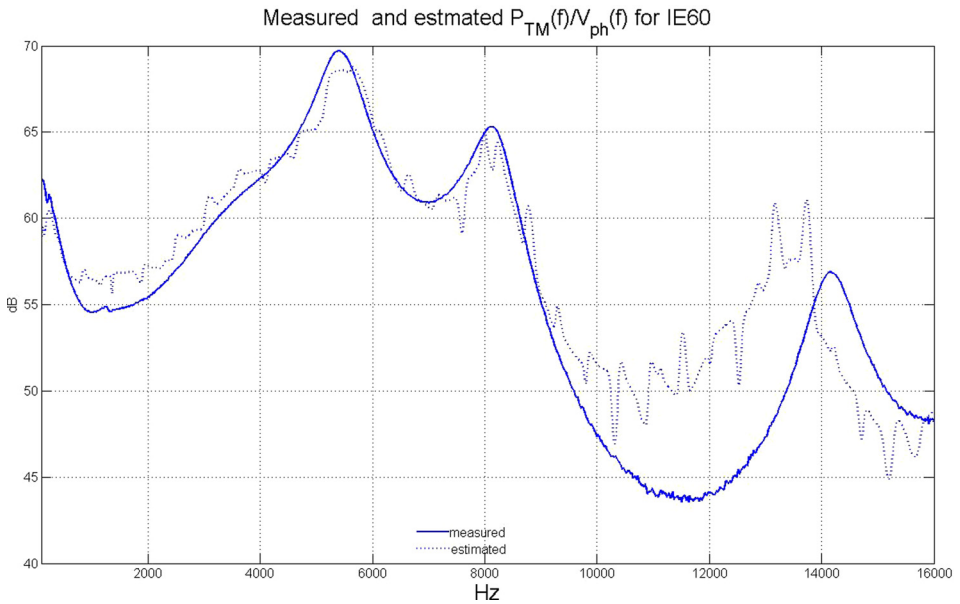

FIG. 13. (Color online) The frequency response of the transfer function from the input of Sennheiser IE60 to the sound pressure signal at the eardrum center estimated (dotted line) given the model ear canal with $L = 2$ mm, and the one measured on a GRAS 45 BM ear simulator (solid line).

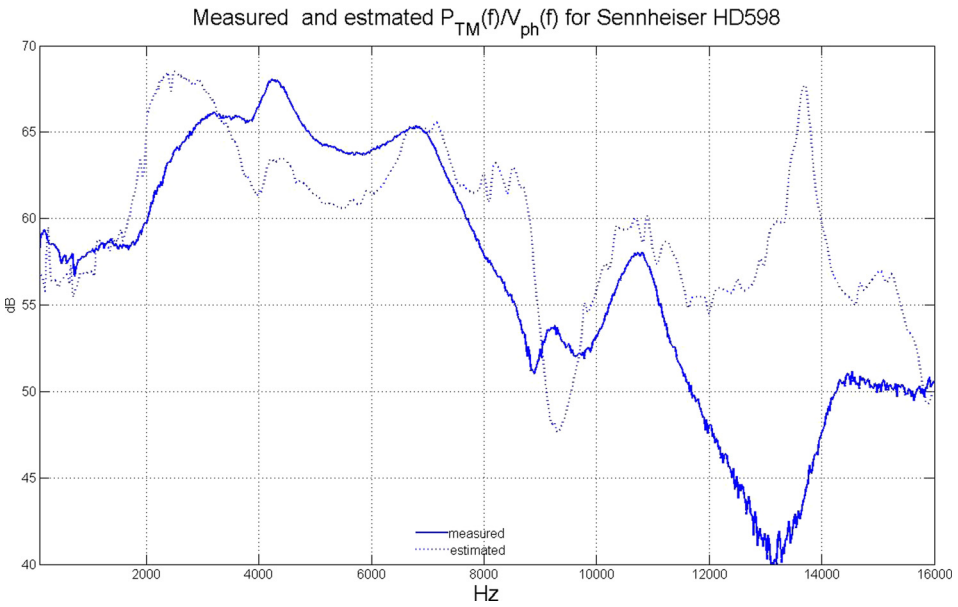

FIG. 14. (Color online) The frequency response of the transfer function from the input of Sennheiser HD 598 to the sound pressure signal at the eardrum center estimated (dotted line) given the model ear canal with $L = 2$ mm, and the one measured on a GRAS 45 BM ear simulator (solid line).

with the inverse of the sweep signal, respectively. The resultant impulse responses are aligned in time and truncated to the same length $N = 500$. respectively, to obtain their frequency responses $P_0(f)$ and $P_{TM}(f)$. The frequency response of the miniature microphone is calibrated with a B&K4189 microphone in an anechoic room, and the measured frequency response $P_0(f)$ is corrected.

It is found that the $P_{TM}(f)/P_0(f)$ estimated for the ear canal area function with the first 12 sectional lengths being $L = 1.9$ mm (total length being $12 \times 1.9 + 4 = 26.8$ mm) (solid line in Fig. 12) is most close to the one measured on HATS (dotted line in Fig. 12) below 10 kHz, which is the specified frequency range of the standard ear simulator. The difference could be mainly due to the difference between the pinna radiation impedance simulated by the AITP (which uses a flat plate to simulate the curved cheek and head area around the pinna) and that simulated by the dummy head. Above 10 kHz, the current standard ear simulator does not simulate a human ear, and also its eardrum impedance is not specified in this range (IEC, 2010). This explains the difference observed above 10 kHz between the $P_{TM}(f)/P_0(f)$ measured on the ear simulator and the one estimated based on the realistic eardrum impedance Z_{TM2}. It is noted that the standard ear simulator effectively simulates a model ear canal with total length about 26.8 mm.

B. The transfer function from headphone input to the eardrum

The H_{ph2TM} frequency responses of IE 60 and of Sennheiser HD 598 are measured on the GRAS 45 BM dummy head with standard small pinna simulators connected to IEC 60318-4 ear simulators, and are plotted using solid lines in Figs. 13 and 14, respectively. The measurements are made by playing a sweep tone signal from 20 Hz to 20 kHz from the headphone under test coupled to the pinna of the dummy head and analyzing the sound signal received at the built-in microphone in the ear simulator using the B&K PULSE program.

For the IE 60 insert headphone, up to 10 kHz, it is found that the H_{ph2TM} frequency response estimated given the model ear canal (dotted line in Fig. 13) matches the measured one (solid line in Fig. 13). For HD 598, the H_{ph2TM} frequency response estimated given the model ear canal (dotted line in Fig. 14) approximates to the measured one below 10 kHz (the specified frequency range of IEC 60318-4 standard ear simulators). The difference between the estimated and measured ones could be reduced if the head and cheek area around the pinna of the AITP is simulated more realistically so that the equivalent sound sources of circumaural headphones can be measured in a more realistic condition.

VIII. CONCLUSION

The present work develops a method of modeling and estimating the frequency responses of acoustic transfer functions of external ears with or without headphones (Secs. II and III). In estimating the frequency response of the transfer function from the input of a headphone to the sound pressure at the eardrum center, it first determines the equivalent sound source and reflection coefficient of the headphone to the ear using the acoustic impedance tube (Secs. V and VI) and then estimates that frequency response based on the acoustic model taking into both effects of the external ear and the headphone on the sound at the eardrum.

The estimation reveals that eardrum impedances affect the resonance peaks and frequencies of the external-ear transfer functions (Fig. 5), whereas ear canal shapes and lengths mainly affect the resonance frequencies of the transfer functions (Figs. 6–8). It also shows that the frequency response of the headphone-to-eardrum transfer function is more consistent across different ear canals for the open headphone Sennheiser HD 598 than for the noise-isolating headphone Sennheiser IE 60 (Figs. 7 and 8). Such combined effects caused by differences in headphone and ear canal cannot be revealed using current standard ear simulators. The good agreements between estimated and measured results validate

that the present method of modeling and estimating external-ear transfer functions with or without headphones can produce estimates comparable to measured ones given realistic external ear and headphone parameters (Sec. VII). A feasible method for obtaining the parameters of human external ears required in the estimation is under research.

The present method can help predict the effects of external ears and headphones on the perceived sounds for a large population and is expected to have applications in audiometric or psychoacoustic measurements, headphone or hearing aid system design, and binaural sound reproduction to estimate and compensate for the effects of external ears and headphones or hearing aids on perceived sounds.

ACKNOWLEDGMENT

This work is supported by Strategic Priority Research Program of the Chinese Academy of Sciences under Grant No. XDA06040501. The authors thank Liguo Wei for helping construct the acoustic tube used in this work.

Boden, H., and Abom, M. (**1986**). "Influence of errors on the two-microphone method for measuring acoustic properties in ducts," J. Acoust. Soc. Am. **79**, 541–549.

Deng, H., Ward, R. M., Beddoes, M., and Hodgson, M. (**2006**). "A new method for obtaining accurate estimates of vocal-tract filters and glottal waves from speech signals," IEEE Trans. Audio Speech Lang. Proc. **14**, 445–455.

Deng, H., and Yang, J. (**2014**). "Simulating external-ear transfer functions," in *21th International Conference on Sound and Vibrations*, July 2014, Beijing, China.

Golub, G. H., and Loan, C. F. V. (**2013**). *Matrix Computations*, 4th ed. (The Johns Hopkins University Press, Baltimore, MD), 290 pp.

Harmmershøi, D., and Møller, H. (**1996**). "Sound transmission to and within the human ear canal," J. Acoust. Soc. Am. **100**(1), 408–427.

Hiipakka, M. (**2011**). "Estimating pressure and volume velocity in the ear canal for insert headphones," in *Proceedings of the International Conference on Acoustics, Speech and Signal Processing*, May 21–22, Honolulu, HI, pp. 289–292.

Hiipakka, M., Kinnari, T., and Pulkki V. (**2012**). "Estimating head-related transfer functions of human subjects from pressure-velocity measurements," J. Acoust. Soc. Am. **131**, 4051–4061.

Hudde, H., and Engel, A. (**1996**). "A wide-band precision acoustic measuring head," Acust. acta Acust. **82**, 895–904.

Hudde, H., and Engel, A. (**1998a**). "Measuring and modeling basic properties of the human middle ear and ear canal. Part I: Model structure and measuring techniques," Acust. acta Acust. **84**, 720–738.

Hudde, H., and Engel, A. (**1998b**). "Measuring and modeling basic properties of the human middle ear and ear canal. Part II: Ear canal, middle ear cavities, eardrum, and ossicles," Acust. acta Acust. **84**, 894–913.

Hudde, H., and Engel, A. (**1998c**). "Measuring and modeling basic properties of the human middle ear and ear canal. Part III: Eardrum impedances, transfer functions and model calculations," Acust. acta Acust. **84**, 1091–1109.

Hudde, H., Engel, A., and Lodwig, A. (**1999**). "Method for estimating the sound pressure at the eardrum," J. Acoust. Soc. Am. **106**, 1977–1992.

IEC (**2010**). IEC 60318-4, *Electroacoustics—Simulators of Human Head and Ear. Part 4: Occluded-Ear Simulator for the Measurement of Earphones Coupled to the Ear by Means of Ear Inserts* (International Electrotechnical Commission, Geneva, Switzerland).

ISO (**1998**). ISO 10534-2, *Acoustics—Determination of Sound Absorption Coefficient and Impedance in Impedance Tubes–Part 2: Transfer-Function Method* (International Organization for Standardization, Geneva, Switzerland), 1998-11-15.

Kinsler, L. E., Frey, A., and Sanders, J. V. (**2000**). *Fundamentals of Acoustics* (Wiley and Sons, New York), pp. 272–291.

Mehrgardt, S., and Mellert, V. (**1977**). "Transformation characteristics of the external human ear," J. Acoust. Soc. Am. **61**(6), 1567–1576.

Møller, H., Hammersøi, D., Jensen, C. B., and Sorensen, M. F. (**1995**). "Transfer characteristics of headphones measured on human ears," J. Audio Eng. Soc. **43**(4), 203–217.

Rabiner, L., and Schafer, R. W. (**2011**). *Theory and Applications of Digital Speech Processing* (Pearson Education, Landisville, PA).

Shaw, E. A. G. (**1975**). "The external ear: New knowledge," Scand. Audiol. Suppl. **5**, 24–50.

Stinson, M. (**1985**). "The spatial distribution of sound pressure within scaled replicas of the human ear canal," J. Acoust. Soc. Am. **78**(5), 1596–1602.

Stinson, M. (**1990**). "Revision of estimates of acoustic energy reflectance at the human eardrum," J. Acoust. Soc. Am. **88**, 1773–1778.

Stinson, M., and Daigle, G. (**2010**). "An eardrum simulator for use with physical replicas of the human ear canal," J. Acoust. Soc. Am. **127**, 1868.

Stinson, M. R., and Daigle, G. A. (**2005**). "Comparison of an analytic horn equation approach and a boundary element method for the calculation of sound fields in the human ear canal," J. Acoust. Soc. Am. **118**, 2405–2411.

Stinson, M. R., and Lawton, B. W. (**1989**). "Specification of the geometry of the human ear canal for the prediction of sound–pressure level distribution," J. Acoust. Soc. Am. **85**, 2492–2503.

Voländer, M. (**2000**). "Acoustic load on the ear caused by headphones," J. Acoust. Soc. Am. **107**, 2082–2088.

Voss, S. E., Rosowski, J. J., Shera, C. A., and Peake, W. T. (**2000**). "Acoustic mechanisms that determine the ear-canal sound pressures generated by earphones," J. Acoust. Soc. Am. **107**, 1548–1565.

Walsh, T., Demkowicz, L., and Charles, R. (**2004**). "Boundary element modeling of the external human auditory system," J. Acoust. Soc. Am. **115**, 1033–1043.